

## Spin-nematic squeezing for dynamical quantum phase transitions in a spinor Bose-Einstein condensate

Yixiao Huang,<sup>1</sup> Yi Ding<sup>1</sup>, Jiahao Xu,<sup>1</sup> Jianning Liu,<sup>1</sup> Hailong Wang,<sup>1</sup> and Heng-Na Xiong<sup>2,\*</sup>

<sup>1</sup>*School of Science, Zhejiang University of Science and Technology, Hangzhou, Zhejiang, 310023, China*

<sup>2</sup>*Department of Applied Physics, Zhejiang University of Technology, Hangzhou 310023, China*



(Received 9 February 2022; accepted 3 August 2022; published 24 August 2022)

We study spin-nematic squeezing in a spinor Bose-Einstein condensate and use it to probe dynamical quantum phase transitions. We show that the quench dynamics of the spin-nematic squeezing exhibits a nonanalytical change with respect to a final quadratic Zeeman energy, and demonstrate that the squeezing detects not only the ground state phase diagram, but also the excited state quantum phase transition. We further analyze the dynamic stabilization of the system and present its relation to the dynamical quantum phase transitions. Our results are applicable to the spinor condensates with both of the sodium and rubidium atoms.

DOI: [10.1103/PhysRevA.106.022430](https://doi.org/10.1103/PhysRevA.106.022430)

### I. INTRODUCTION

Nonequilibrium quantum many-body dynamics have been widely studied in various physical systems, such as trapped ions [1,2], Rydberg atoms [3], and ultracold atoms [4–6]. A central direction of this field that concerns new manifestations of various critical phenomena is dynamical quantum phase transitions (DQPTs). Generally, the DQPTs denote nonanalyticities in the evolution of an initially equilibrated state undergoing a sudden change of a system parameter [7–9]. A spinor Bose-Einstein condensate provides a good platform to study the nonequilibrium dynamics which shows many interesting phenomena, such as spin domains [10–14], topological defects [15–19], the Kibble-Zurek mechanism [15,20–29], and DQPTs. In a recent experiment of the spinor condensate, DQPTs based on ground state phase transitions were observed [30]. The DQPTs were also detected in the spinor condensate corresponding to an excited state phase diagram [31,32]. However, these two phenomena were observed by starting with two different initial states, respectively. Thus it is still an open question whether the DQPTs could be observed with probing both to the ground state phase diagram and the excited state quantum phase transition by starting with the same initial state, instead of two different ones.

Spin squeezing in nonequilibrium quantum many-body dynamics has seen rapid progress in recent years due to its critical role in quantum information, entanglement detection [33–38], and high-precision measurement [39–55]. Squeezed states were usually specified by three different components of the total spin vector  $\hat{\mathbf{S}}(\hat{S}_x, \hat{S}_y, \hat{S}_z)$ . While in a spinor Bose-Einstein condensate, the state is specifically expressed in the SU(3) Cartesian dipole quadrupole basis which consists of the three components of spin vector and the nematic tensor  $\hat{Q}_{i,j}(i, j \in \{x, y, z\})$ . The nematic moments in matrix form can be written as  $\hat{Q}_{i,j} = \hat{S}_i \hat{S}_j + \hat{S}_j \hat{S}_i - \frac{4}{3} \delta_{i,j}$  with  $\delta_{i,j}$  being the Kronecker delta. The presence of the nematic tensor in-

dicates that the squeezing can be generated by some other types of correlations beyond the spin-spin correlation, such as the spin-nematic or internematic correlations [53–57]. The spin-nematic squeezing has been experimentally observed in the spinor condensate [58].

In this paper, we investigate the connection between the spin-nematic squeezing and the DQPTs in an antiferromagnetic spinor condensate with sodium atoms. We use the spin-nematic squeezing to characterize the behaviors of the DQPTs. The squeezing detects not only the ground state phase transition, but also the phase transition for the highest energy level. We prepare the condensate in a polar state where all of the atoms condense in the  $m_F = 0$  state. We find the quench dynamics of the spin-nematic squeezing shows a nonanalytical change as a function of the quadratic Zeeman energy of a final Hamiltonian at  $q = 0$  and  $q = -2c_2$  ( $c_2$  denotes an interaction strength). Here  $q = 0$  and  $q = -2c_2$  are the critical points for the ground phase transition between the antiferromagnetic (AFM) phase and the polar phase, and the transition between the polar phase and a broken axisymmetry (BA) state for the highest energy level, respectively. We analyze the dynamic stabilization of the system and show the relation with the DQPTs. We further confirm that the dynamical fractional population and the optimal squeezing time are also good measures of the DQPTs. Finally, we discuss the dynamics of the squeezing with an initial state as AFM state, and show that squeezing starting with the AFM and the polar states exhibit an asymmetric behavior around the final Zeeman energy  $q = 0$ . Although our results are obtained in the case of  $c_2 > 0$ , it could be easily generalized to  $c_2 < 0$ . We hope our results could be experimentally verified by both of the condensates with sodium ( $c_2 > 0$ ) and rubidium ( $c_2 < 0$ ) atoms.

### II. SPIN-NEMATIC SQUEEZING OF THE SPINOR CONDENSATE

We consider a spinor Bose-Einstein condensate with an external magnetic field. In a single-mode approximation (SMA),

\*xiongna@zjut.edu.cn

the Hamiltonian of the system takes the form [59,60]

$$\hat{H} = \frac{c_2}{2N} \hat{S}^2 + \sum_{m_F=-1}^1 (qm_F^2 - pm_F) \hat{a}_{m_F}^\dagger \hat{a}_{m_F}, \quad (1)$$

where  $\hat{S}$  is total spin operator,  $N$  is the total particle number of the system,  $m_F = -1, 0, 1$  being the magnetic spin quantum number,  $q$  and  $p$  denote the quadratic and linear Zeeman energy, respectively. The operator  $\hat{a}_j$  ( $\hat{a}_j^\dagger$ ) being an annihilation (creation) operator of the  $j$ th spin mode and  $c_2$  is the spin-dependent interaction energy. The parameter  $c_2 > 0$  and  $c_2 < 0$  correspond to the sodium and rubidium atoms, respectively. In the following, we consider the case of  $c_2 > 0$ . First, we notice the magnetization  $\hat{S}_z = \hat{a}_1^\dagger \hat{a}_1 - \hat{a}_{-1}^\dagger \hat{a}_{-1}$  is conserved during the time evolution, i.e.,  $[\hat{H}, \hat{S}_z] = 0$ . Thus the dynamical evolution is restricted to a subspace with a fixed eigenvalue of  $\hat{S}_z$ . To start with, all the atoms are prepared in the  $m_F = 0$  mode, the system will be in the subspace with the zero magnetization, and the effective Hamiltonian is reduced to

$$\hat{H} = \frac{c_2}{2N} \hat{S}^2 - q \hat{a}_0^\dagger \hat{a}_0. \quad (2)$$

The dynamical properties of the system are closely related to the ratio  $q/c_2$ .

According to the definition of the nematic tensors, the operators  $\hat{Q}_{i,j}$  are written as [61–63]

$$\begin{aligned} \hat{Q}_{yz} &= \frac{i}{\sqrt{2}} (\hat{a}_0^\dagger \hat{a}_{-1} - \hat{a}_1^\dagger \hat{a}_0 + \hat{a}_0^\dagger \hat{a}_1 - \hat{a}_{-1}^\dagger \hat{a}_0), \\ \hat{Q}_{xz} &= \frac{1}{\sqrt{2}} (\hat{a}_1^\dagger \hat{a}_0 - \hat{a}_0^\dagger \hat{a}_{-1} + \hat{a}_0^\dagger \hat{a}_1 - \hat{a}_{-1}^\dagger \hat{a}_0), \\ \hat{Q}_{xx} &= \frac{2}{3} \hat{a}_0^\dagger \hat{a}_0 - \frac{1}{3} (\hat{a}_1^\dagger \hat{a}_1 + \hat{a}_{-1}^\dagger \hat{a}_{-1}) + \hat{a}_1^\dagger \hat{a}_{-1} + \hat{a}_{-1}^\dagger \hat{a}_1, \\ \hat{Q}_{yy} &= \frac{2}{3} \hat{a}_0^\dagger \hat{a}_0 - \frac{1}{3} (\hat{a}_1^\dagger \hat{a}_1 + \hat{a}_{-1}^\dagger \hat{a}_{-1}) - \hat{a}_1^\dagger \hat{a}_{-1} - \hat{a}_{-1}^\dagger \hat{a}_1, \\ \hat{Q}_{zz} &= \frac{2}{3} \hat{a}_1^\dagger \hat{a}_1 - \frac{4}{3} \hat{a}_0^\dagger \hat{a}_0 + \frac{2}{3} \hat{a}_{-1}^\dagger \hat{a}_{-1}. \end{aligned}$$

The operators  $\{\hat{S}_x, \hat{Q}_{yz}, \hat{Q}_+\}$  and  $\{\hat{S}_y, \hat{Q}_{xz}, \hat{Q}_-\}$  comprise two SU(2) subspaces. Here,  $\hat{Q}_+$  and  $\hat{Q}_-$  are defined as  $\hat{Q}_+ = \hat{Q}_{zz} - \hat{Q}_{yy}$ ,  $\hat{Q}_- = \hat{Q}_{xx} - \hat{Q}_{zz}$ , respectively. From the generalized Heisenberg uncertainty relation  $\Delta \hat{A} \Delta \hat{B} \geq \frac{1}{2} |\langle [\hat{A}, \hat{B}] \rangle|$ , only operator pairs with non-zero expectation values for their commutation relations, i.e.,  $[\hat{A}, \hat{B}] \neq 0$ , can exhibit squeezing. Considering an initial state with all of the atoms condensed in the  $m_F = 0$  mode, we find that only two operators  $\hat{Q}_\pm$  have nonzero expectation values. Based on these relations, two different spin-nematic squeezing parameters are defined in terms of quadratures of the operators [58,63]

$$\xi_{x(y)}^2 = 2 \langle [\Delta (\cos \theta \hat{S}_{x(y)} + \sin \theta \hat{Q}_{yz(xz)})]^2 \rangle / |\langle \hat{Q}_{+(-)} \rangle| \quad (3)$$

with  $\theta$  being the quadrature angle. The parameter  $\xi_{x(y)}^2 < 1$  indicates the spin-nematic squeezing. For a proper  $\theta$ , we can obtain a minimum value of  $\xi_{x(y)}^2$ . Focusing on the squeezing parameter  $\xi_x^2$ , a minimum value of  $\xi_x^2$  is obtained at a proper

$\theta$  and given by

$$\xi_x^2 = \frac{A - \sqrt{B^2 + C^2}}{|\langle \hat{Q}_+ \rangle|}, \quad (4)$$

where  $A \equiv \langle \hat{S}_x^2 + \hat{Q}_{yz}^2 \rangle$ ,  $B \equiv \langle \hat{S}_x^2 - \hat{Q}_{yz}^2 \rangle$ , and  $C \equiv \langle \hat{S}_x \hat{Q}_{yz} + \hat{Q}_{yz} \hat{S}_x \rangle$ .

We consider a short time evolution and thus the initial condensate in the mode  $m_F = 0$  will be weakly affected by the spin-mixing dynamics. Such a condition is called the undepleted pump approximation. In this approximation, the operators  $\hat{a}_0$  and  $\hat{a}_0^\dagger$  are replaced by the  $c$  number  $\sqrt{N}$ . We define three operators  $\hat{K}_x = \frac{1}{2} (\hat{a}_1^\dagger \hat{a}_{-1}^\dagger + \hat{a}_1 \hat{a}_{-1})$ ,  $\hat{K}_y = \frac{1}{2i} (\hat{a}_1^\dagger \hat{a}_{-1}^\dagger - \hat{a}_1 \hat{a}_{-1})$ , and  $\hat{K}_z = \frac{1}{2} (\hat{a}_1^\dagger \hat{a}_1 + \hat{a}_{-1}^\dagger \hat{a}_{-1} + 1)$  which satisfy  $[\hat{K}_x, \hat{K}_y] = -i\hat{K}_z$ ,  $[\hat{K}_y, \hat{K}_z] = i\hat{K}_x$ , and  $[\hat{K}_z, \hat{K}_x] = i\hat{K}_y$ , and belong to the SU(1,1) group [64–66]. The effective Hamiltonian (with constant terms dropped) becomes

$$\begin{aligned} \hat{H}_{\text{eff}} &= 2c_2 \hat{K}_x + 2[c_2 - c_2/(2N) + q] \hat{K}_z \\ &\approx 2c_2 \hat{K}_x + 2(c_2 + q) \hat{K}_z. \end{aligned} \quad (5)$$

In the undepleted pump approximation, we have

$$\begin{aligned} A &= 4N \langle \hat{K}_z \rangle = 2N \frac{-\beta^2 + \alpha^2 \cosh \sqrt{\alpha^2 - \beta^2} t}{(\alpha^2 - \beta^2)}, \\ B &= 4N \langle \hat{K}_x \rangle = \frac{-4N\alpha\beta \sinh^2 \frac{\sqrt{\alpha^2 - \beta^2} t}{2}}{\alpha^2 - \beta^2}, \\ C &= 4N \langle \hat{K}_y \rangle = \frac{2N\alpha \sinh \sqrt{\alpha^2 - \beta^2} t}{\sqrt{\alpha^2 - \beta^2}}, \end{aligned} \quad (6)$$

where  $\alpha = 2c_2$  and  $\beta = 2(c_2 + q)$ . At the critical points  $q_f = 0$  and  $q_f = -2c_2$ , we have  $\alpha^2 = \beta^2$ , thus the above parameters reduce to  $A = 2N(1 + \alpha^2 t^2/2)$ ,  $B = -N\alpha^2 t^2$ , and  $C = 2N\alpha t$ , respectively. A direct calculation from Eq. (6) yields a relationship  $\langle \hat{K}_z \rangle^2 = \langle \hat{K}_x \rangle^2 + \langle \hat{K}_y \rangle^2 + \frac{1}{4}$ . The squeezing parameter in Eq. (5) is reduced to

$$\xi_x^2 \approx 2 \langle \hat{K}_z \rangle - \sqrt{4 \langle \hat{K}_z \rangle^2 - 1}. \quad (7)$$

In Fig. 1, we plot the spin-nematic squeezing parameter  $10 \log_{10}(\xi_x^2)$  and  $\mathcal{N}_0 \equiv \langle \hat{N}_0 \rangle / N$  as a function of  $t$  for different  $q/c_2$ . We find  $\mathcal{N}_0 \approx 1$  in Figs. 1(a) and 1(c), which indicates the small population transfers from the  $m_F = 0$  mode to other modes. For such a case, the results of the squeezing obtained by numerical calculation from the Hamiltonian in Eq. (2) coincide well with the analytical one in Eq. (7), see Figs. 1(d) and 1(f). When the value of  $\mathcal{N}_0$  is a little far away from 1, the analytical result is no longer valid since the undepleted pump approximation breaks down, see Figs. 1(b) and 1(e).

### III. SIGNATURES OF DYNAMICAL QUANTUM PHASE TRANSITIONS

First, we introduce the phase diagram of the system. Since we neglect the linear Zeeman energy, the ground state of the system is determined by the value of  $q/c_2$ . As shown in Fig. 2 (a<sub>1</sub>), the ground state for sodium atoms with  $c_2 > 0$  exhibits a first-order quantum transition at the critical point  $q = 0$  from polar phase where all atoms condense in the  $m_F = 0$  mode to

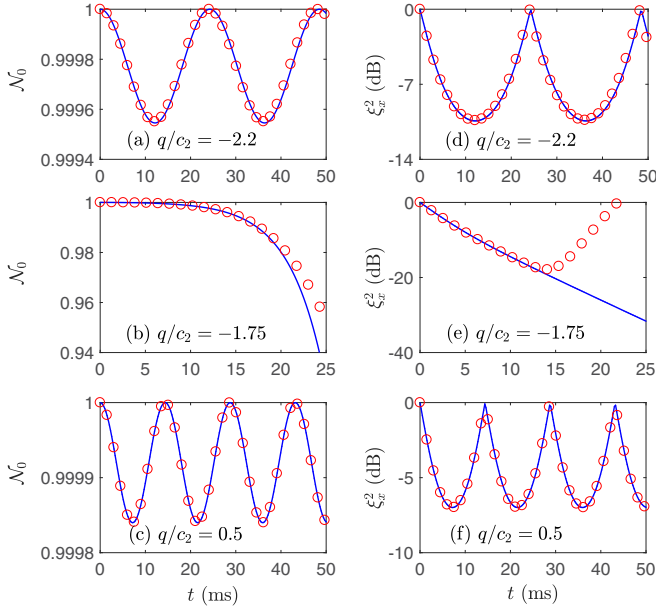


FIG. 1. The particle population in the mode  $m_F = 0$  (a)–(c) and spin-nematic squeezing  $\xi_x^2$  (d)–(f) as a function of  $t$  for different  $q/c_2$ . The red circles are the numerical results and the blue solid lines correspond to the analytical results shown in Eq. (7). The total particle number of the system is chosen  $N = 10^4$  and the interaction strength  $c_2/h = 31$  Hz.

an AFM phase with equally populated atoms in the  $m_F = \pm 1$  modes [30]. In Fig. 2(a<sub>2</sub>), we can find the highest energy level exhibits a phase transition which is similar to rubidium atoms with  $c_2 < 0$ , where a second order phase transition occurs at  $q = 2c_2$  between a BA phase with nonzero population at the  $m_F = 0$  mode and the AFM phase. Another transition occurs at  $q = -2c_2$  between a BA phase and a polar phase [31,67,68].

To explore the DQPTs, we quench the quadratic Zeeman energy after generating the initial state. Starting with a high fixed magnetic field, the initial state is prepared to be  $|N_1, N_{-1}, N_0\rangle = |0, 0, N\rangle$ . Then a microwave dressing field is suddenly turned on to abruptly change  $q_B$  to  $q_f = q_B + q_M$ , where  $q_B$  and  $q_M$  represent the initial quadratic Zeeman energy induced by a magnetic field and a microwave dressing field, respectively. The quadratic Zeeman energy induced by the magnetic field can only introduce a positive net quadratic  $q_B \propto B^2 > 0$ , while the quadratic Zeeman shift can be swept from  $-\infty$  to  $\infty$  by the microwave dressing field. Generally, the DQPTs were experimentally observed by measuring the fractional population [30–32,69,70]. Here, we use the spin-nematic squeezing to probe the DQPTs.

We define a quantity,  $\xi_m^2 \equiv \min_t(\xi_x^2)$ , being the optimal squeezing. We denote the occurrence time of the optimal squeezing as the optimal time  $t_m$  and the fractional population at  $t_m$  as  $\mathcal{N}_0^m$ . In the regions of  $q_f < -2c_2$  and  $q_f > 0$ ,  $\xi_m^2$  can be obtained as

$$\xi_m^2 = \begin{cases} \frac{q_f}{q_f + 2c_2}, & q_f > 0, \\ \frac{q_f + 2c_2}{q_f}, & q_f < -2c_2. \end{cases} \quad (8)$$

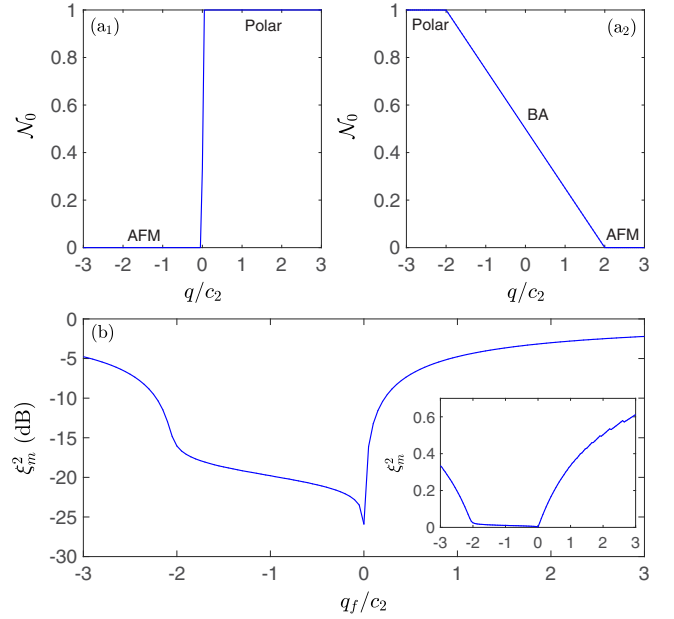


FIG. 2. The order parameter  $\mathcal{N}_0$  as a function of the quadratic Zeeman energy  $q$  in the units of  $c_2$  for the ground state (a<sub>1</sub>) and the highest energy state with zero magnetization (a<sub>2</sub>). Numerical result of the optimal spin-nematic squeezing  $\xi_m^2$  (b) with  $c_2/h = 31$  Hz. The inset shown in (b) denotes the squeezing parameter  $\xi_m^2$  without Logarithmic function. The particle number of the system is chosen  $N = 10^4$ .

Moreover, one can get the optimal squeezing time  $t_m = \frac{\pi}{2\sqrt{q_f(q_f + 2c_2)}}$  and the corresponding fractional population  $\mathcal{N}_0^m = \frac{2c_2^2}{q_f(q_f + 2c_2)}$  in both of the above two regions. In Fig. 2(b), we plot  $\xi_m^2$  as a function of  $q_f/c_2$ . It shows qualitatively different behaviors in the three regions of  $q_f/c_2$ . The location of the singularity at  $q_f = 0$  in the squeezing parameter coincides with that of ground state phase transition.

The squeezing parameter  $\xi_m^2$  also presents a discontinuous change at  $q_f = -2c_2$  which corresponds to the critical point of excited state phase transition, see the inset shown in Fig. 2(b). In fact, the spin squeezing parameter will get sharper with increasing of the system size. As shown in Fig. 3, this feature turns up at both of the two points  $q_f = -2c_2$  and  $q_f = 0$ .

Figures 4 further illustrates  $\mathcal{N}_0^m$  and the optimal evolution time  $t_m$  with respect to  $q_f$ , respectively. We find  $\mathcal{N}_0^m$  exhibits a decrease at  $q_f = -2c_2$  and a sudden dip at  $q_f = 0$ . The optimal time  $t_m$  shows a sharp peak around  $q_f = 0$  and  $q_f = -2c_2$ . Here, the optimal time is closely related to the nearest-neighbor energy gap at the highest two energy levels of the system, see Appendix A. This is why it could be used to capture the excited state phase transition in the antiferromagnetic condensate.

Physically, the above phenomena can also be explained in terms of the phase diagram of the system and the stabilization dynamics in the mean-field approximation. As shown in Figs. 2(a<sub>1</sub>) and 2(a<sub>2</sub>), the highest energy state for  $q < -2c_2$  and the ground state for  $q > 0$  share the same polar state with  $\mathcal{N}_0 = 1$ . Starting from the polar state, the population

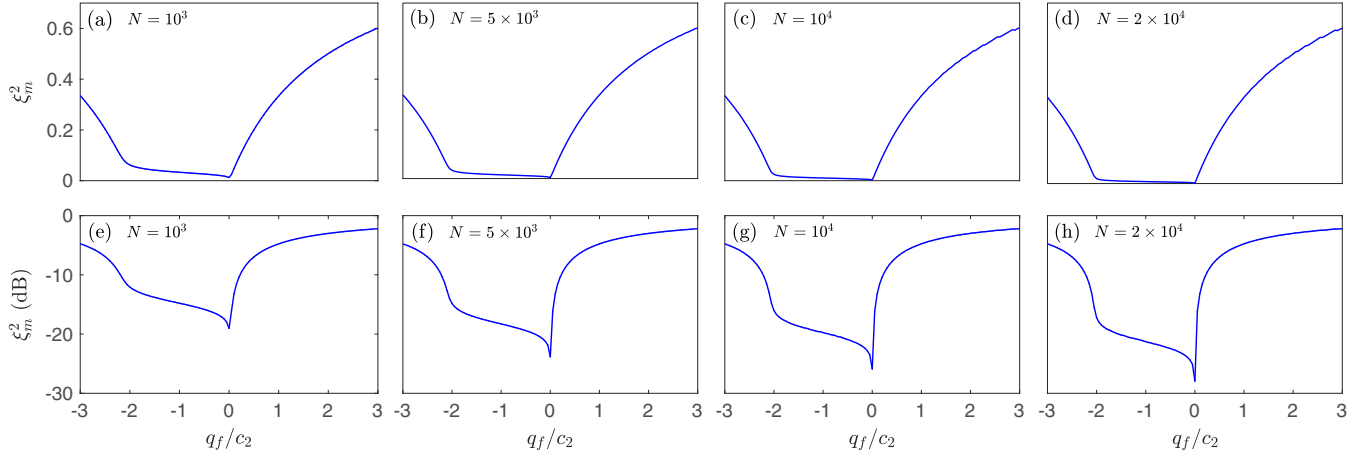


FIG. 3. The optimal spin-nematic squeezing  $\xi_m^2$  (a)–(d) and  $10 \log_{10} \xi_m^2$  (e)–(h) as a function of  $q_f/c_2$  for different  $N$  with  $c_2/h = 31$  Hz.

in the mode  $m_F = 0$  remains  $N$  when we suddenly tune  $q$  to  $q_f < -2c_2$  or  $q_f > 0$ . When we tune  $q$  to the region of  $-2c_2 < q_f < 0$ , many particles will be transferred from the  $m_F = 0$  mode to the  $m_F = \pm 1$  modes. Indeed, according to the stability analysis, the dynamics of the system are stable in the regions of  $q_f < -2c_2$ , and  $q_f > 0$ , thus  $\mathcal{N}_0^m \simeq 1$  and  $\xi_m^2$  in these two regions is much smaller than  $\xi_m^2$  in the region of  $-2c_2 < q_f < 0$ . The analytic stability region is derived in Appendix B.

In a current experiment [30], the signatures of DQPT at  $q_f = 0$  was observed by measuring the value of  $\mathcal{N}_0$  at the first dip of the spin oscillations induced by the spin mixing dynamics. But with the same measurement of  $\mathcal{N}_0$ , the DQPT at  $q_f = -2c_2$  was not detected in the experiment. This is because, in the practical experiment, the spin oscillation at  $q_f = -2c_2$  is barely visible in quench dynamics and one could not find where the first dip is located. To test whether the measurement of the squeezing at  $q_f = -2c_2$  will encounter the similar problem in the experiment, we plot  $\xi_x^2$  and  $\mathcal{N}_0$  as a function of  $t$  with  $q_f = -2c_2$  in Fig. 5. It is shown the squeezing parameter  $\xi_x^2$  attains its minimum at  $t = 18.6$  ms which is about half of the time of the first dip. That is, one could observe the minimum squeezing before the spin oscillation goes to its first dip. Thus both of DQPTs at  $q_f = 0$  and  $q_f = -2c_2$  can be observed by measuring  $\xi_m^2$ .

On the contrary, starting from the initial AFM state  $|N/2, N/2, 0\rangle$ , the signature of DQPT at  $q_f = 2c_2$  is experi-

mentally observed by measuring  $\mathcal{N}_0$  at the first peak of the spin oscillation, while  $q_f = 0$  cannot be observed [32]. Here, both of the two critical points can be observed by measuring the spin-nematic squeezing. As shown in Fig. 6,  $\xi_m^2$  is plotted as a function of  $q_f/c_2$  with the initial state  $|N/2, N/2, 0\rangle$ . Comparing the result shown in Fig. 2(b), we find the curves of  $\xi_m^2$  for the initial states  $|N/2, N/2, 0\rangle$  and  $|0, 0, N\rangle$  are asymmetric around  $q_f = 0$ . In order to explain such a phenomenon, we consider the undepleted pump approximation in which the particle numbers in the modes  $m_F = \pm 1$  are weakly affected by the spin mixing dynamics. We assume the operator  $\hat{a}_{\pm 1}$  and  $\hat{a}_{\pm 1}^\dagger$  are replaced by the  $c$  number  $\sqrt{N/2}$ . Then the SU(1,1) operators are redefined as  $\hat{K}'_x = \frac{1}{4}(\hat{a}_0^\dagger \hat{a}_0^\dagger + \hat{a}_0 \hat{a}_0)$ ,

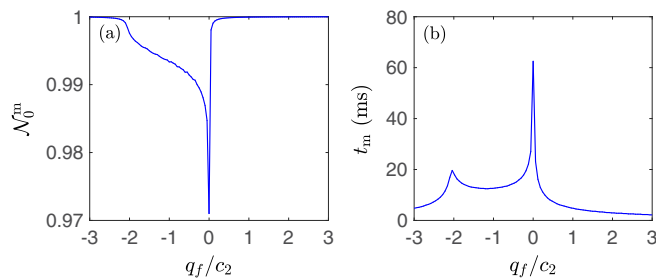


FIG. 4. Numerical result of the fractional population at  $t_m$ , i.e.,  $\mathcal{N}_0^m$  (a), and  $t_m$  (b) as a function of  $q_f/c_2$  with  $c_2/h = 31$  Hz. The particle number of the system is chosen  $N = 10^4$ .

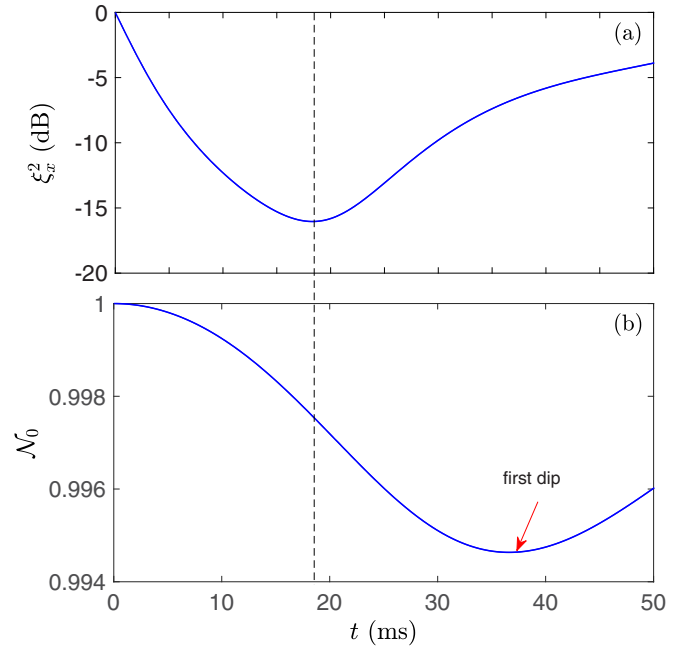


FIG. 5. The numerical results of the spin-nematic squeezing  $\xi_x^2$  (a) and the fractional population  $\mathcal{N}_0$  (b) as a function of  $t$  with  $q_f = -2c_2$ . The red arrow denotes the position of the first dip of the spin oscillations. The vertical dotted line indicates the optimal squeezing occurs. The parameters are the same as for Fig. 1.

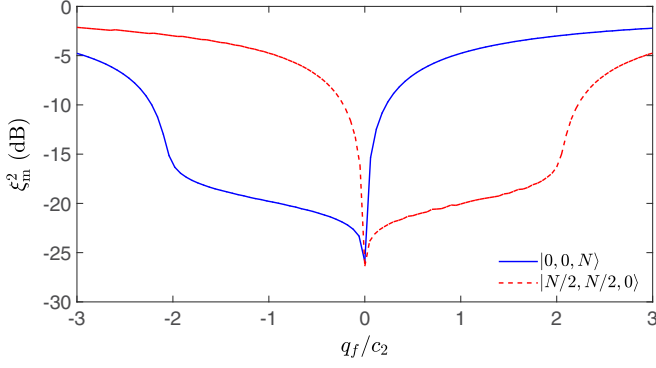


FIG. 6. The numerical results of the optimal spin-nematic squeezing  $\xi_m^2$  as a function of  $q_f/c_2$  with the initial state  $|N/2, N/2, 0\rangle$  and  $|0, 0, N\rangle$ , respectively. The parameters are the same as for Fig. 1.

$\hat{K}'_y = \frac{1}{4i}(\hat{a}_0^\dagger \hat{a}_0^\dagger - \hat{a}_0 \hat{a}_0)$ , and  $\hat{K}'_z = \frac{1}{2} \hat{a}_0^\dagger \hat{a}_0 + \frac{1}{4}$ , the Hamiltonian in Eq. (2) becomes

$$\hat{H}'_{\text{eff}} = 2c_2 \hat{K}'_x + 2(c_2 - q) \hat{K}'_z. \quad (9)$$

Here we notice that the difference between the effective Hamiltonians in Eqs. (5) and (9) is the sign of  $q$ . Thus the dynamics of optimal spin-nematic squeezing  $\xi_m^2$  exhibits an asymmetrical behavior around  $q_f = 0$ . In fact, our results can also be applied to the case of rubidium atoms which have negative  $c_2$ . When  $c_2 < 0$ ,  $\xi_m^2$  for the initial state as  $|0, 0, N\rangle$  is the same as  $\xi_m^2$  for the initial state as  $|N/2, N/2, 0\rangle$  with  $c_2 > 0$ .

#### IV. CONCLUSION

In summary, we have studied the spin-nematic squeezing in a spinor condensate with sodium atoms, and showed that the spin-nematic squeezing can be used to characterize the DQPTs of the spinor condensate. The squeezing detects both the ground phase transition between the AFM phase and polar phase and the excited state transition between the polar phase and the BA phase. We also showed the dynamical fractional population at the optimal squeezing time could also distinguish the DQPTs. We further made a connection between dynamical stabilization and the nonanalytical change of the spin-nematic squeezing. Finally, we discussed the dynamics of the squeezing for an AFM state as the initial state, and found the optimal squeezing  $\xi_m^2$  starting with the AFM and the polar states exhibit an asymmetrical behavior around  $q_f = 0$ . In addition, our results are correct for both of the cases of  $c_2 > 0$  and  $c_2 < 0$ . Thus both of the condensates with sodium ( $c_2 > 0$ ) and rubidium atoms ( $c_2 < 0$ ) are good candidates for experimental verification.

#### ACKNOWLEDGMENTS

This work was supported by the Natural Science Foundation of Zhejiang Province through Grant No. LY22A050002 and the Fundamental Research Funds for the Provincial Universities of Zhejiang (Grant No. RF-A2020002).

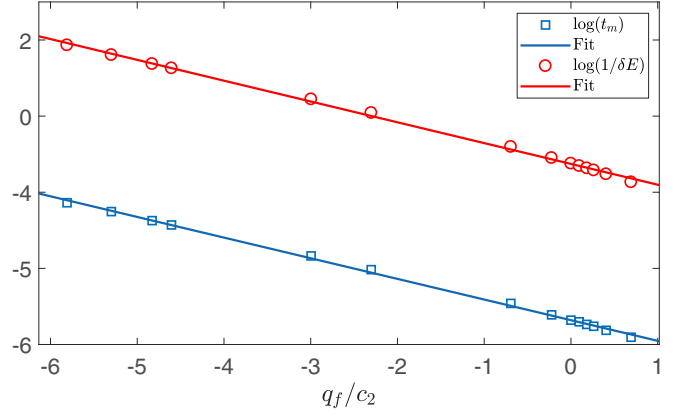


FIG. 7. Power-law scaling of the optimal time  $t_m$  and the dip time  $\tau$  (the inverse of the relevant energy gap) in a log-log diagram. The extracted critical exponents for  $t_m$  and  $\tau$  are, respectively,  $-0.5467$  and  $-0.5424$ , based on linear fits (denoted by solid lines) to the log-log curves.

#### APPENDIX A: POWER-LAW SCALING OF THE OPTIMAL TIME AND THE ENERGY GAP

To understand why the time scale can characterize DQPT, we discuss the relationship between the optimal time and the energy gap  $\delta E$  at the highest two energy levels of the system. In Fig. 7, we plot  $t_m$  and  $\tau = 1/\delta E$  as a function of  $q_f/c_2$ . We find the results exhibit a power-law scaling with  $q_f/c_2$  and the two log-log curves have similar slopes. The extracted power-law scaling exponents are  $-0.5467$  for  $t_m$  and  $-0.5424$  for  $\tau$  through linear fits to the log-log curves. This implies that the optimal time  $t_m$  is closely related to  $\delta E$  in the energy spectrum. So it can capture excited state phase transitions of the system.

#### APPENDIX B: DYNAMIC STABILIZATION OF THE SPINOR CONDENSATE

Here we derive the dynamical stability regions of the spinor condensate. In the mean-field framework and under the SMA, the wave functions for the different spin components are represented by a complex vector  $\vec{\zeta} = (\zeta_1, \zeta_0, \zeta_{-1})^T$ , where  $\zeta_i$  is the amplitude and satisfies  $|\vec{\zeta}|^2 = 1$ . Considering an initial state with zero fractional magnetization, the magnetization will be a constant in the motion. The vector  $\zeta_i$  can be written as

$$\begin{aligned} \zeta_1 &= \sqrt{\frac{1-\rho_0}{2}} e^{i(\theta+\theta_L)}, & \zeta_0 &= \sqrt{\rho_0}, \\ \zeta_{-1} &= \sqrt{\frac{1-\rho_0}{2}} e^{i(\theta-\theta_L)}, \end{aligned} \quad (B1)$$

where  $\rho_i = N_i/N$  denotes the spin population in  $i$ th component,  $\theta = (\theta_1 + \theta_{-1} - 2\theta_0)/2$  is the relative phase between spinors, and  $\theta_L = (\theta_1 - \theta_{-1})/2$  is the Larmor recession phase. The free spin mixing dynamics yields the equations [71]

$$\begin{aligned} \dot{\rho}_0 &= 2\tilde{c}_2 \rho_0 (1 - \rho_0) \sin 2\theta, \\ \dot{\theta} &= -2\tilde{q} + 2\tilde{c}_2 (1 - 2\rho_0) (1 + \cos 2\theta), \end{aligned} \quad (B2)$$

where  $\tilde{c}_2 = c_2/\hbar$  and  $\tilde{q} = q/\hbar$ . To analysis the stability regions, we discuss the dynamical equations of the spin and nematic operators. Using the parametrization shown in Eq. (B1), the expectation values of  $\hat{S}_x$ ,  $\hat{Q}_{yz}$ ,  $\hat{S}_y$ , and  $\hat{Q}_{xz}$  for the vector  $\zeta_i$  are obtained as [62]

$$\begin{aligned} S_x &= 2\sqrt{\rho_0(1-\rho_0)} \cos\theta \cos\theta_L, \\ Q_{yz} &= -2\sqrt{\rho_0(1-\rho_0)} \sin\theta \cos\theta_L, \\ S_y &= -2\sqrt{\rho_0(1-\rho_0)} \cos\theta \sin\theta_L, \\ Q_{xz} &= -2\sqrt{\rho_0(1-\rho_0)} \sin\theta \sin\theta_L. \end{aligned}$$

Defining  $S_\perp^2 = S_x^2 + S_y^2$ ,  $Q_\perp^2 = Q_{yz}^2 + Q_{xz}^2$ , we have  $S_\perp = 2\sqrt{\rho_0(1-\rho_0)} \cos\theta$  and  $Q_\perp = 2\sqrt{\rho_0(1-\rho_0)} \sin\theta$ . Further define a parameter  $x = 2\rho_0 - 1$ , we obtain

$$S_\perp^2 + Q_\perp^2 + x^2 = 1. \quad (\text{B3})$$

Obviously,  $S_\perp$ ,  $Q_\perp$ , and  $x$  form a unit sphere and can be denoted as a spin representation. Based on the Eq. (B2), the differential equations of  $S_\perp$  and  $Q_\perp$  are [62]

$$\begin{pmatrix} \dot{S}_\perp \\ \dot{Q}_\perp \end{pmatrix} = \begin{bmatrix} 0 & \tilde{q}_f \\ -(2\tilde{c}_2 + \tilde{q}_f) & 0 \end{bmatrix} \begin{pmatrix} S_\perp \\ Q_\perp \end{pmatrix}. \quad (\text{B4})$$

To solve the dynamical stability of the system, we employ a linear stability analysis which has a wide application in various nonlinear systems. To begin with, three infinitesimal variables  $\delta S_\perp$ ,  $\delta Q_\perp$  and  $\delta x$  are introduced by  $S_\perp = S_\perp^0 + \delta S_\perp$ ,  $Q_\perp = Q_\perp^0 + \delta Q_\perp$ , and  $x = x^0 + \delta x$ , respectively, where  $S_\perp^0$ ,  $Q_\perp^0$  and  $x^0$  are the expectation of the initial state. For our case with the initial state as  $\rho_0 = 1$ , we have  $S_\perp^0 = Q_\perp^0 = 0$  and  $x^0 = 1$ . Then the linearized equations of motion in the matrix form reduce to

$$\begin{pmatrix} \delta \dot{S}_\perp \\ \delta \dot{Q}_\perp \end{pmatrix} = \begin{bmatrix} 0 & \tilde{q}_f \\ -(2\tilde{c}_2 + \tilde{q}_f) & 0 \end{bmatrix} \begin{pmatrix} \delta Q_\perp \\ \delta S_\perp \end{pmatrix}. \quad (\text{B5})$$

Defining the above matrix as  $\mathbf{m}$ , the time evolution is given by its exponential form as  $\exp(t\mathbf{m})$ . Adopting the stability analysis technique employed in an optical resonator theory, the determinant of the dynamics of  $S_\perp$  and  $Q_\perp$  must satisfy the condition  $|\text{Tr}[\exp(t\mathbf{m})]| < 2$ . A direct calculation yields

$$|\cosh \sqrt{-\tilde{q}_f(2\tilde{c}_2 + \tilde{q}_f)}t| < 1. \quad (\text{B6})$$

Obviously, the above equation holds when  $q_f > 0$  and  $q_f < -2c_2$  for  $c_2 > 0$ . Thus the dynamic of the system is stable in the region of  $q_f > 0$  and  $q_f < -2c_2$ .

- 
- [1] J. Zhang, G. Pagano, P. W. Hess, A. Kyprianidis, P. Becker, H. Kaplan, A. V. Gorshkov, Z.-X. Gong, and C. Monroe, *Nature (London)* **551**, 601 (2017).
- [2] P. Jurcevic, H. Shen, P. Hauke, C. Maier, T. Brydges, C. Hempel, B. P. Lanyon, M. Heyl, R. Blatt, and C. F. Roos, *Phys. Rev. Lett.* **119**, 080501 (2017).
- [3] H. Bernien, S. Schwartz, A. Keesling, H. Levine, A. Omran, H. Pichler, S. Choi, A. S. Zibrov, M. Endres, M. Greiner, V. Vuletić, and M. D. Lukin, *Nature (London)* **551**, 579 (2017).
- [4] N. Fläschner, D. Vogel, M. Tarnowski, B. S. Rem, D.-S. L. ühmann, M. Heyl, J. C. Budich, L. Mathey, K. Sengstock, and C. Weitenberg, *Nat. Phys.* **14**, 265 (2018).
- [5] W. Sun, C.-R. Yi, B.-Z. Wang, W.-W. Zhang, B. C. Sanders, X.-T. Xu, Z.-Y. Wang, J. Schmiedmayer, Y. Deng, X.-J. Liu, S. Chen, and J.-W. Pan, *Phys. Rev. Lett.* **121**, 250403 (2018).
- [6] S. Smale, P. He, B. A. Olsen, K. G. Jackson, H. Sharum, S. Trotzky, J. Marino, A. M. Rey, and J. H. Thywissen, *Sci. Adv.* **5**, eaax1568 (2019).
- [7] M. Heyl, *Rep. Prog. Phys.* **81**, 054001 (2018).
- [8] A. A. Zvyagin, *Low Temp. Phys.* **42**, 971 (2016).
- [9] B. Žunkovič, A. Silva, and M. Fabrizio, *Philos. Trans. R. Soc. A* **374**, 20150160 (2016).
- [10] S. R. Leslie, J. Guzman, M. Vengalattore, J. D. Sau, M. L. Cohen, and D. M. Stamper-Kurn, *Phys. Rev. A* **79**, 043631 (2009).
- [11] M. Vengalattore, J. Guzman, S. R. Leslie, F. Serwane, and D. M. Stamper-Kurn, *Phys. Rev. A* **81**, 053612 (2010).
- [12] J. Kronjäger, C. Becker, P. Soltan-Panahi, K. Bongs, and K. Sengstock, *Phys. Rev. Lett.* **105**, 090402 (2010).
- [13] J. Guzman, G.-B. Jo, A. N. Wenz, K. W. Murch, C. K. Thomas, and D. M. Stamper-Kurn, *Phys. Rev. A* **84**, 063625 (2011).
- [14] C. V. Parker, L. Ha, and C. Chin, *Nat. Phys.* **9**, 769 (2013).
- [15] L. E. Sadler, J. M. Higbie, S. R. Leslie, M. Vengalattore, and D. M. Stamper-Kurn, *Nature (London)* **443**, 312 (2006).
- [16] L. S. Leslie, A. Hansen, K. C. Wright, B. M. Deutsch, and N. P. Bigelow, *Phys. Rev. Lett.* **103**, 250401 (2009).
- [17] J. Y. Choi, W. J. Kwon, and Y. I. Shin, *Phys. Rev. Lett.* **108**, 035301 (2012).
- [18] J.-Y. Choi, W. J. Kwon, M. Lee, H. Jeong, K. An, Y.-I. Shin, *New J. Phys.* **14**, 053013 (2012).
- [19] L.-Y. Qiu, H.-Y. Liang, Y.-B. Yang, H.-X. Yang, T. Tian, Y. Xu, L.-M. Duan, *Sci. Adv.* **6**, eaba7292 (2020).
- [20] E. M. Bookjans, A. Vinit, and C. Raman, *Phys. Rev. Lett.* **107**, 195306 (2011).
- [21] A. Vinit, E. M. Bookjans, C. A. R. Sá de Melo, and C. Raman, *Phys. Rev. Lett.* **110**, 165301 (2013).
- [22] T. M. Hoang, M. Anquez, B. A. Robbins, X. Y. Yang, B. J. Land, C. D. Hamley, and M. S. Chapman, *Nat. Commun.* **7**, 11233 (2016).
- [23] M. Anquez, B. A. Robbins, H. M. Bharath, M. Boguslawski, T. M. Hoang, and M. S. Chapman, *Phys. Rev. Lett.* **116**, 155301 (2016).
- [24] J. H. Kim, S. W. Seo, and Y. Shin, *Phys. Rev. Lett.* **119**, 185302 (2017).
- [25] M. Prüfer, P. Kunkel, H. Strobel, S. Lannig, D. Linnemann, C.-M. Schmied, J. Berges, T. Gasenzer, and M. K. Oberthaler, *Nature (London)* **563**, 217 (2018).
- [26] S. Kang, S. W. Seo, H. Takeuchi, and Y. Shin, *Phys. Rev. Lett.* **122**, 095301 (2019).
- [27] K. Jiménez-García, A. Invernizzi, B. Evrard, C. Frapolli, J. Dalibard, and F. Gerbier, *Nat. Commun.* **10**, 1422 (2019).
- [28] Z. Chen, T. Tang, J. Austin, Z. Shaw, L. Zhao, and Y. Liu, *Phys. Rev. Lett.* **123**, 113002 (2019).
- [29] S. Kang, D. Hong, J. H. Kim, and Y. Shin, *Phys. Rev. A* **101**, 023613 (2020).
- [30] H.-X. Yang, T. Tian, Y.-B. Yang, L.-Y. Qiu, H.-Y. Liang, A.-J. Chu, C. B. Dağ, Y. Xu, Y. Liu, and L.-M. Duan, *Phys. Rev. A* **100**, 013622 (2019).

- [31] C. B. Dağ, S.-T. Wang, and L.-M. Duan, *Phys. Rev. A* **97**, 023603 (2018).
- [32] T. Tian, H.-X. Yang, L.-Y. Qiu, H.-Y. Liang, Y.-B. Yang, Y. Xu, and L.-M. Duan, *Phys. Rev. Lett.* **124**, 043001 (2020).
- [33] A. S. Sørensen and K. Mølmer, *Phys. Rev. Lett.* **86**, 4431 (2001).
- [34] J. K. Korbicz, J. I. Cirac, and M. Lewenstein, *Phys. Rev. Lett.* **95**, 120502 (2005).
- [35] J. K. Korbicz, O. Gühne, M. Lewenstein, H. Haffner, C. F. Roos, and R. Blatt, *Phys. Rev. A* **74**, 052319 (2006).
- [36] G. Tóth, C. Knapp, O. Gühne, and H. J. Briegel, *Phys. Rev. A* **79**, 042334 (2009).
- [37] L. Pezzé and A. Smerzi, *Phys. Rev. Lett.* **102**, 100401 (2009).
- [38] P. Hyllus, L. Pezzé, A. Smerzi, and G. Tóth, *Phys. Rev. A* **86**, 012337 (2012).
- [39] D. J. Wineland, J. J. Bollinger, W. M. Itano, F. L. Moore, and D. J. Heinzen, *Phys. Rev. A* **46**, R6797(R) (1992).
- [40] D. J. Wineland, J. J. Bollinger, W. M. Itano, and D. J. Heinzen, *Phys. Rev. A* **50**, 67 (1994).
- [41] A. Sørensen, L.-M. Duan, J. Cirac, and P. Zoller, *Nature (London)* **409**, 63 (2001).
- [42] D. Leibfried, M. Barrett, T. Schaetz, J. Britton, J. Chiaverini, W. Itano, J. Jost, C. Langer, and D. Wineland, *Science* **304**, 1476 (2004).
- [43] C. Gross, T. Zibold, E. Nicklas, J. Esteve, and M. K. Oberthaler, *Nature (London)* **464**, 1165 (2010).
- [44] M. F. Riedel, P. Böhi, Y. Li, T. W. Hänsch, A. Sinatra, and P. Treutlein, *Nature (London)* **464**, 1170 (2010).
- [45] I. D. Leroux, M. H. Schleier-Smith, and V. Vuletić, *Phys. Rev. Lett.* **104**, 073602 (2010).
- [46] A. Louchet-Chauvet, J. Appel, J. J. Renema, D. Oblak, N. Kjaergaard, and E. S. Polzik, *New J. Phys.* **12**, 065032 (2010).
- [47] V. Giovannetti, S. Lloyd, and L. Maccone, *Nat. Photonics* **5**, 222 (2011).
- [48] C. Lee, J. Huang, H. Deng, H. Dai, and J. Xu, *Front. Phys.* **7**, 109 (2012).
- [49] R. J. Sewell, M. Koschorreck, M. Napolitano, B. Dubost, N. Behbood, and M. W. Mitchell, *Phys. Rev. Lett.* **109**, 253605 (2012).
- [50] E. Yukawa, G. J. Milburn, C. A. Holmes, M. Ueda, and K. Nemoto, *Phys. Rev. A* **90**, 062132 (2014).
- [51] J. G. Bohnet, K. C. Cox, M. A. Norcia, J. M. Weiner, Z. Chen, and J. K. Thompson, *Nat. Photonics* **8**, 731 (2014).
- [52] R. J. Lewis-Swan, M. A. Norcia, J. R. K. Cline, J. K. Thompson, and A. Maria Rey, *Phys. Rev. Lett.* **121**, 070403 (2018).
- [53] S. J. Masson, M. D. Barrett, and S. Parkins, *Phys. Rev. Lett.* **119**, 213601 (2017).
- [54] D. Kajtoch and E. Witkowska, *Phys. Rev. A* **93**, 023627 (2016).
- [55] Q.-S. Tan, Y. Huang, Q.-T. Xie, and X. Wang, *Phys. Rev. A* **102**, 043307 (2020).
- [56] D. Linnemann, H. Strobel, W. Muessel, J. Schulz, R. J. Lewis-Swan, K. V. Kheruntsyan, and M. K. Oberthaler, *Phys. Rev. Lett.* **117**, 013001 (2016).
- [57] Ö. E. Müstecaplıoğlu, M. Zhang, and L. You, *Phys. Rev. A* **66**, 033611 (2002).
- [58] C. D. Hamley, C. S. Gerving, T. M. Hoang, E. M. Bookjans, and M. S. Chapman, *Nat. Phys.* **8**, 305 (2012).
- [59] Y. Kawaguchi and M. Ueda, *Phys. Rep.* **520**, 253 (2012).
- [60] D. M. Stamper-Kurn and M. Ueda, *Rev. Mod. Phys.* **85**, 1191 (2013).
- [61] C. S. Gerving, T. M. Hoang, B. J. Land, M. Anquez, C. D. Hamley, and M. S. Chapman, *Nat. Commun.* **3**, 1169 (2012).
- [62] T. M. Hoang, C. S. Gerving, B. J. Land, M. Anquez, C. D. Hamley, and M. S. Chapman, *Phys. Rev. Lett.* **111**, 090403 (2013).
- [63] Y. Huang, H. N. Xiong, Z. Sun, and X. Wang, *Phys. Rev. A* **92**, 023622 (2015).
- [64] B. Yurke, S. L. McCall, and J. R. Klauder, *Phys. Rev. A* **33**, 4033 (1986).
- [65] K. Wodkiewicz and J. Eberly, *J. Opt. Soc. Am. B* **2**, 458 (1985).
- [66] M. Gabbriellini, L. Pezzè, and A. Smerzi, *Phys. Rev. Lett.* **115**, 163002 (2015).
- [67] Z. Zhang and L.-M. Duan, *Phys. Rev. Lett.* **111**, 180401 (2013).
- [68] Y. Liu, E. Gomez, S. E. Maxwell, L. D. Turner, E. Tiesinga, and P. D. Lett, *Phys. Rev. Lett.* **102**, 225301 (2009).
- [69] B. Žunkovič, M. Heyl, M. Knap, and A. Silva, *Phys. Rev. Lett.* **120**, 130601 (2018).
- [70] P. Titum, J. T. Iosue, J. R. Garrison, A. V. Gorshkov, and Z. X. Gong, *Phys. Rev. Lett.* **123**, 115701 (2019).
- [71] W. Zhang, D. L. Zhou, M.-S. Chang, M. S. Chapman, and L. You, *Phys. Rev. A* **72**, 013602 (2005).